The computation of directional selectivity in the retina occurs presynaptic to the ganglion cell

Lyle J. Borg-Graham

Unité de Neurosciences Intégrative et Computationnelles, UPR CNRS 2191-INAF CNRS, 91198 Gif-sur-Yvette, France

Correspondence should be addressed to L.J.B.-G.(lyle@cogni.iaf.cnrs-gif.fr)

Directional selectivity is a response that is greater for a visual stimulus moving in one (PREF) direction than for the opposite (NULL) direction, and its computation in the vertebrate retina is a classical issue in functional neurophysiology. To date, most quantitative experimental studies have relied on extracellular responses for identifying properties of the directionally selective circuit. Here I describe an intracellular analysis using whole-cell patch recordings of the synaptic events underlying the spike response in directionally selective ganglion cells of the turtle retina. These quantitative measurements allowed me to distinguish among various explicit classes of circuit models that can, in principle, account for ganglion cell directional selectivity. I found that ganglion cell directional selectivity is due to an excitatory input that itself is directionally selective, and that the crucial shunting inhibition implicated in this computation must act on cells presynaptic to the ganglion cell.

The cellular architecture and mechanisms underlying retinal directional selectivity have long been an active area of research[1] (for review, see ref. 2), and a basic question is where this computation arises within the retina. Although early models of this computation focused on interactions in the outer retina[3], more recent work has concentrated on the properties of directionally selective ganglion cells and their afferent inputs[4–8].

Three basic combinations of synaptic input to a neuron can produce a directionally selective spike response (**Fig. 1**). A parsimonious view from the directionally selective ganglion cell implies that the selectivity either arises from within the cell (a postsynaptic model), or is already present in the inputs to the cell (a presynaptic model). The postsynaptic model requires at least an interaction between spatially separated inputs, with a delay. Pharmacological evidence as to the fundamental involvement of $GABA_A$ receptor-mediated inhibition[9–12] suggests that this interaction is between an inhibitory and excitatory input. Thus, the spatial separation and temporal asymmetry between the inputs are such that for motion in the NULL direction, excitation and inhibition arrive synchronously, canceling each other[13]. In the PREF direction, excitation arrives out of phase with inhibition, thus allowing a suprathreshold excitatory postsynaptic potential (EPSP). An important aspect of this scheme is that the computation of directional selectivity occurs at the ganglion cell; neither the excitation nor inhibition by themselves need depend on stimulus direction.

There are two basic versions of a presynaptic model. In the first, the excitatory input is non-directional with the inhibitory input stronger for the NULL direction stimulus (inhibitory-NULL model). In the second version, a non-directional inhibitory input is coupled with an excitatory input that is stronger for the PREF stimulus (excitatory-PREF model). Typical intrinsic postsynaptic nonlinearities may make the directionality of the spike output quantitatively different than directionality of the integrated synaptic response. For example, up to some maximum value, the spike threshold will tend to increase the directionality, whereas spike saturation will tend to decrease the directionality. Nevertheless, in both presynaptic models, the fundamental computation of directionality occurs before the ganglion cell.

The postsynaptic and two presynaptic models have distinct biophysical signatures in terms of the excitatory, $G_{ex}(t)$, and inhibitory, $G_{inh}(t)$, synaptic conductance inputs onto the directionally selective ganglion cell. These inputs may be estimated from the modulation of the ganglion cell's input conductance during the visual response, $G(t)$, and the apparent reversal potential of the evoked input, $E_{rev}(t)$[14]. An upper bound estimate on the excitatory synaptic input may also be made from the evoked current under voltage clamp, $I(t)$, provided the holding potential is sufficiently negative to suppress or reverse any inhibitory synaptic current. Furthermore, the finding that $GABA_A$ receptor-mediated inhibition operates primarily by shunting the membrane resistance[14–16] facilitates model predictions in terms of the peak, average and duration of $G(t)$, relative to the resting condition, G_0. I analyzed the three directional selectivity models in terms of the theoretical predictions of directionally selective ganglion cell responses for PREF and NULL stimuli. I then examined experimental data from the turtle retina to discriminate among the models. I found that the excitatory input to directionally selective ganglion cells was itself directionally selective, and that the inhibitory input to these neurons was insufficient to account for the postsynaptic computation of directional selectivity.

Results

Model predictions

I derived quantitative values (**Table 1**) for the models' predictions using a simple steady-state isopotential neuron (for the pre- and postsynaptic models) and a postsynaptic model based on a reconstructed ganglion cell with a detailed, passive dendritic tree

Table 1. Comparison of predictions by post- and presynaptic models of directional selectivity with experimental measures of synaptic dynamics during PREF and NULL responses of directionally selective retinal ganglion cells.

Synaptic measure	Postsynaptic model		Presynaptic models		Experimental value
	Isopotential	Dendritic	Inhibitory-NULL	Excitatory-PREF	
D_{G*ex}	0	0.03	0	≥0	0.20 ± 0.009***
D_{Gex}	0	0.03	0	≥0	0.22 ± 0.008***
D_{G*inh}	0	–0.05	≤0	0	0.11 ± 0.016**
D_{Ginh}	0	0.02	≤0	0	0.06 ± 0.018*
D_{I*}	0	–0.14	0	≥0	0.17 ± 0.005***
D_{I}	0	0.03	0	≥0	0.17 ± 0.006***
PREF G*(t)	≥160%	180%	≥130%	≥130%	156 ± 1.6%
NULL G*(t)	≥190%	220%	≥190%	N/A	143 ± 1.6%
D_{G*}	<0	–0.09	≤0	≥0	0.14 ± 0.011***
D_{G}	0	0.03	≤0	≥0	0.15 ± 0.009***
D_{T}	>0	0.24	≤0	≥0	–0.04 ± 0.012*

For the various pairs of peak and average directional indices (D_{G*ex} and D_{Gex}, D_{G*inh} and D_{Ginh}, D_{I*} and D_{I}, D_{G*} and D_{G} for the estimated excitatory synaptic conductance, the estimated inhibitory synaptic conductance, the voltage clamp current at hyperpolarized holding potentials 1(t), and the somatic input conductance G(t), respectively), the predicted inequality for each presynaptic model requires that at least one of the indices be non-zero. G*(t) is the peak value of G(t). D_T is the directional index for the PREF and NULL durations of G(t). Predictions for the two presynaptic models are for an isopotential cell. Experimental values are expressed as the average ± s.e.m. For non-zero value for directional indices, ***p < 0.01, **p < 0.05, *p < 0.20. Values of D_{I*} and D_{I} are derived for the dendritic model from a holding potential of –90 mV, and for the other models from a holding potential of –70 mV. N/A, not applicable.

(**Fig. 2**). The detailed model allowed for lower bound estimates of conductance changes measured at the soma, given the inherent sublinear synaptic integration within dendrites[16,17]. These predictions may be expressed as specific values for G(t) and in terms of a directionality index (D; range, –1 to 1) that compares the PREF versus NULL response. D is positive when the PREF response is larger, negative when the NULL response is larger, and zero for equivalent responses (see Methods).

The most direct predictions concern the relative PREF and NULL strength of $G_{ex}(t)$, I(t) and $G_{inh}(t)$ (directional indices of peaks and averages given by D_{G*ex}, D_{Gex}, D_{I*}, D_{I}, D_{G*inh} and D_{Ginh} in **Table 1**). For the postsynaptic model, $G_{ex}(t)$, I(t) and $G_{inh}(t)$ are independent of stimulus direction. For the inhibitory-NULL model, $G_{ex}(t)$ and I(t) are non-directional with either the peak and/or the average of $G_{inh}(t)$ larger for the NULL response. For the excitatory-PREF model, $G_{inh}(t)$ is non-directional, and either the peaks and/or the averages of $G_{ex}(t)$ and I(t) are larger for the PREF response. Simulations of the detailed postsynaptic model verified these predictions, except for the peak of I(t), which favored the NULL response.

I next considered the total input conductance, G(t). To generate the experimentally observed ganglion cell EPSPs, the PREF

Fig. 1. Three basic combinations of excitatory (○) and inhibitory (●) synaptic input onto a directionally selective neuron can account for the neuron's response properties. The inputs in the postsynaptic model are not directional themselves, but the spatial and temporal shift among them allows a correlation that underlies the suppression of the NULL direction response. On the other hand, for the two presynaptic models, one type of input is itself directionally selective (arrows), whereas its partner is not directionally selective. In principle, each of the three directional selectivity circuit models is sufficient, but not necessarily mutually exclusive. The quantitative predictions presented here assume sufficiency, and the goal of this study was to determine which, if any, of these models are able to explain the data on their own.

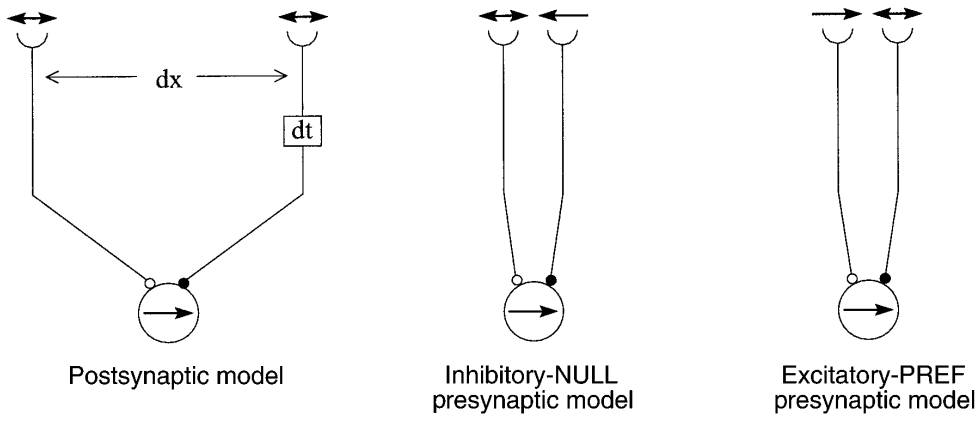

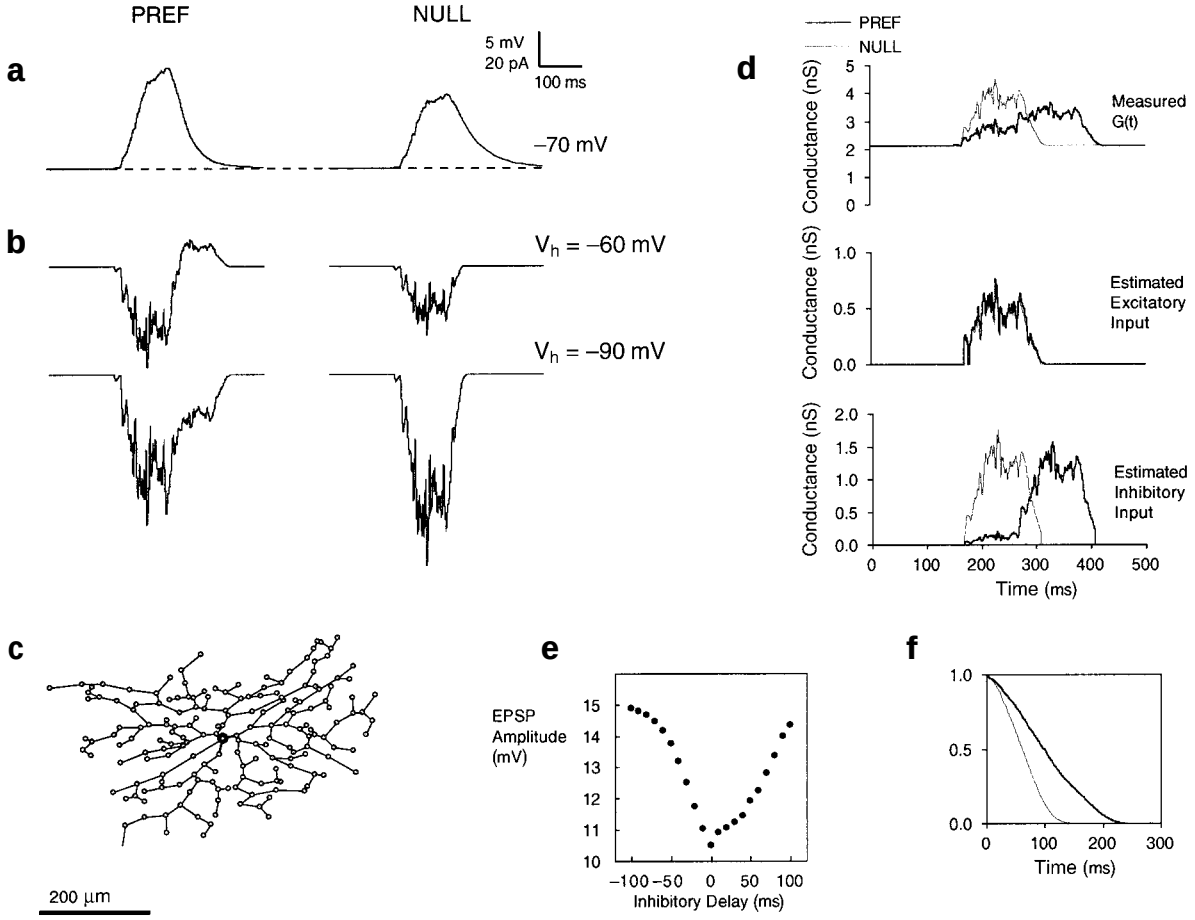

Fig. 2. Compartmental model simulation of postsynaptically generated directional selectivity based on excitatory–inhibitory synaptic correlation at the ganglion cell (**c**, circuit nodes marked by circles). (**a**, **b**) PREF (left) and NULL (right) responses correspond to delays of 100 and 0 ms, respectively, between excitation and inhibition at any given node. Scale applies to (**a**; 5 mV) and (**b**; 20 pA). (**a**) Current-clamp recordings of the soma voltage. (**b**) Somatic voltage clamp traces (V_h = –60 mV, top; –90 mV, bottom). (**d**) Total input conductance, G(*t*), as measured from the soma (top), and dissection of excitatory (middle) and inhibitory (bottom) synaptic input from the voltage clamp records in (**b**). The maximum value of G(*t*) occurs during the NULL response, reaching 220% of G_0. (**e**) Somatic EPSP amplitude as a function of relative delay between excitation and inhibition. (**f**) Normalized autocorrelations of the G(*t*) responses showing greater correlation between the inputs for the NULL response, that is, $T_P > T_N$ (D_T = 0.49).

peak G(*t*) of the presynaptic models must be at least 130% of G_0 (G*(*t*), **Table 1**). To account for inhibition acting on the ganglion cell, the peak NULL G(*t*) for the postsynaptic and inhibitory-NULL models must be at least 190% of the resting conductance G_0. Reflecting the directionality of the input in the presynaptic models, either the peak and/or average G(*t*) of the inhibitory-NULL and excitatory-PREF model is greater for the NULL and PREF responses, respectively (D_{G*} and D_G, **Table 1**). In contrast, for the postsynaptic model, the independence of excitation and inhibition on direction means that the PREF and NULL averages of G(*t*) will be the same, but the NULL peak G(*t*) will be larger, due to the input correlation. Simulations of the dendritic postsynaptic model showed only a small deviation from equivalent PREF and NULL average G(*t*), and confirmed the larger NULL peak G(*t*) (**Table 1** and **Fig. 2**).

The final prediction concerns the dynamics of G(*t*). In the postsynaptic model, the greater correlation between excitation and inhibition during the NULL response means that the duration of G(*t*), T_N, will be shorter than the PREF duration of G(*t*), T_P. This prediction was confirmed by simulations of the dendritic postsynaptic model (D_T, **Table 1**; **Fig. 2d**, top; **Fig. 2f**). The presynaptic models' predictions for T_P and T_N follow those for the PREF/NULL preference of the peak and average of G(*t*), which, in particular, allow T_P to equal T_N.

Electrophysiological measures

To test these predictions, I made whole-cell patch recordings of directionally selective retinal ganglion cells in the turtle (**Figs. 3**, **4** and **5**; population results in **Table 1**). My first finding was that the peak and average of the excitatory input was greater for the PREF response, whether calculated from the conductance and reversal potential modulation ($G_{ex}(t)$, **Figs. 3d**, **4a** and **5d**), or estimated on the basis of hyperpolarized voltage-clamp currents (I(*t*), **Figs. 3b** and **4d**). Surprisingly, overall the inhibitory input $G_{inh}(t)$ was also larger for the PREF response (**Figs. 3d**, **4a** and **5d**). Nevertheless, this input was not sufficient to overcome the PREF excitation.

I then compared the total conductance changes for the PREF and NULL responses. I found that the peaks of G(*t*) during the NULL response, when a postsynaptic action of inhibition would

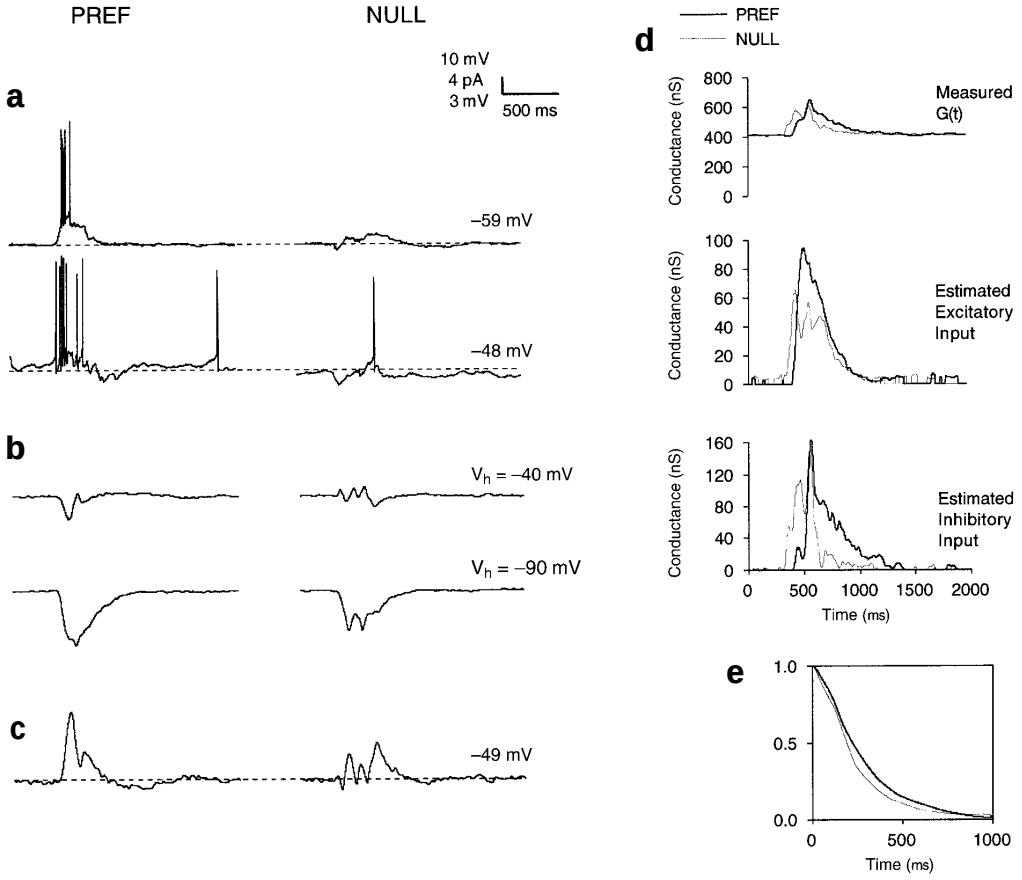

Fig. 3. Electrophysiological recordings of visual responses of a directionally selective ganglion cell (B25) in the turtle retina. Stimulus was a 200 μm spot moving at 4 μm/ms, with PREF directions of 90° (**a**, left) or 122° (**b**, left), and NULL directions of 270° (**a**, right) or 292° (**b**, right). (**a**) Current-clamp recording of directionally selective spiking response without (top) and with (bottom) injected depolarizing current. Directional selectivity is maintained despite membrane depolarization of about 10 mV by current injection, showing that this response property is robust with respect to spike threshold. Scale applies to (**a**, 10 mV) (**b**, 4 pA) and (**c**, 3 mV). (**b**) Voltage-clamp traces (V_h = –40, top; –90 mV, bottom; 4 trials each) low-pass filtered at 200 Hz. (**c**) Reconstruction of current-clamp response from voltage-clamp records. Stability of the responses is indicated by the preserved PREF-NULL distinction. (**d**) Somatic G(*t*) (top) and dissection of excitatory (middle) and inhibitory (bottom) components for the PREF and NULL responses, derived from voltage -clamp recordings in (**b**). Modulation of the input conductance G(*t*) has both greater area (D_G = 0.14) and peak (D_{G*} = 0.09) for the PREF response, and its peak is 59% above G_0. The peak and the integral of both the excitatory and inhibitory components are all larger for the PREF response (D_{G*ex} = 0.11, D_{Gex} = 0.13, D_{G*inh} = 0.15, D_{Ginh} = 0.03). (**e**) Normalized autocorrelation of the G(*t*) waveforms showing that the NULL response is only slighter more correlated than the PREF response (D_T = 0.08).

be expected to be largest, were smaller than predicted by either the postsynaptic or inhibitory-NULL models (**Fig. 4b**; average NULL peak value, 143% relative to G_0). In addition, both the peaks and averages of G(*t*) during the PREF response were significantly larger than those during the NULL response (average PREF peak value, 156% relative to G_0; **Fig. 4b** and **d**). Finally, I compared the PREF and NULL durations of G(*t*); on average, these were slightly longer for the NULL response (**Fig. 4c**).

Discussion

The excitatory input to directionally selective retinal ganglion cells in response to motion was consistently larger for the preferred stimulus. This is the defining characteristic of the excitatory-PREF presynaptic model, and thus argues against the fundamental computation of directional selectivity within ganglion cell dendrites.

Furthermore, my results argue against a critical involvement of synaptic inhibition in directional selectivity at the retinal ganglion cell itself. The size of the shunting input, on the order of 50% of the resting input conductance, was insufficient to account for the observed NULL suppression of excitatory synaptic input. Also, both the peak and average of the overall conductance modulation were larger for the PREF response. Finally, the slightly longer duration of the overall NULL synaptic input versus the PREF input was opposite to what would be expected by a direction-dependent NULL correlation between excitation and inhibition. These observations rule out both the postsynaptic model and the inhibitory-NULL presynaptic model.

Directionally selective inhibition for gain control

In many cells, inhibition is stronger for the PREF response, which would seem to be essentially counterproductive with respect to the task of discriminating stimulus direction. A similar PREF tuning of both excitatory and inhibitory input occurs in directionally selective neurons of the accessory optic system of the turtle (M. Ariel, personal communication). A possible functional involve-

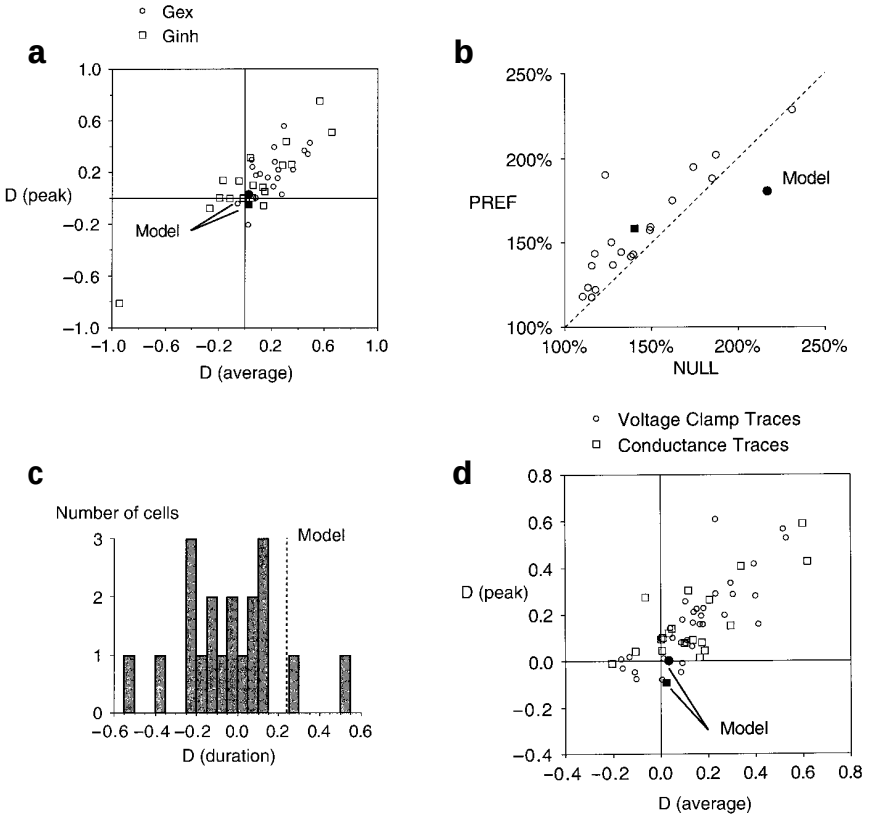

Fig. 4. Population measures for synaptic inputs to directionally selective ganglion cells in the turtle. Model predictions correspond to the detailed postsynaptic model simulations in Fig. 2 (●, for *D* indices of $G_{inh}(t)$ in **a** and of I(*t*) in **d**, and for peak conductance in **b**; ■, for *D* indices of $G_{ex}(t)$ in **a** and of G(*t*) in **d**; – – –, for D_T in **c**). (**a**) *D* indices of peak and average of excitatory and inhibitory components, $G_{ex}(t)$ and $G_{inh}(t)$, calculated from the G(*t*) and $E_{rev}(t)$ responses. These measures tend to be positive, favoring the PREF response, in comparison to the model prediction, which gives very similar PREF and NULL values of the peak and average. The single outlier of inhibitory input strongly biased for the NULL direction nevertheless caused a small peak G(*t*) of about 120% relative to G_0. (**b**) The peak values of G(*t*) for the PREF and NULL responses relative to the resting conductance G_0 (○); average value from data given by filled box. Almost all the measured peaks favor the PREF response, and are smaller than the lower-bound value given by the simulated postsynaptic model, which also favors the NULL response. Dashed line indicates equality. (**c**) D_T, the PREF/NULL directional index of the duration of G(*t*). (**d**) *D* indices of peak and average of I(*t*) (○) and G(*t*) traces (□). The indices for the peak and average of all the measured responses tend to be positive, and thus favor the PREF response. In comparison, the simulated average G(*t*) and the peak and average of I(*t*) are almost equal, and the index for the peak G(*t*) is clearly negative, favoring the NULL response.

ment of this input as a feedforward gain-control mechanism is illustrated in the response to a grating stimulus of an ON directionally selective ganglion cell (**Fig. 5**). The directionally selective current-clamp response to four cycles of the grating is shown in Fig. 5a. (Spikes were lost at this time in the recording.) The underlying conductance changes (**Fig. 5c**) showed strong adaptation (compare the heights and widths of the responses for the first and fourth cycle), and dissection of the conductance traces into excitatory and inhibitory components showed that both adapt (**Fig. 5d**). This balanced adaptation resulted in much less adaptation in the subsequent EPSPs (compare with **Fig. 5a**; also illustrated in the voltage record reconstructed from the voltage-clamp traces, **Fig. 5b**). Indeed, inhibition must decay with excitation to allow a slower decay of the resulting EPSP. If only feedforward pathways are involved, a reasonable assumption for retinal ganglion cells[18], this co-decay requires that inhibition arise at least in part from the directional selectivity circuit presynaptic to the ganglion cell.

Comparison with other studies

A recent study[19] reported whole-cell voltage-clamp measurements of directionally selective ganglion cells of the rabbit retina. The conclusion of the authors of this study was that directional selectivity was produced within the ganglion cell dendrites, that is, the postsynaptic model was supported. PREF/NULL asymmetry of the current responses was increased as the holding potential was increasingly depolarized (thereby reducing the driving force for excitation). This asymmetry went to zero when the intracellular concentration of Cl^- was equilibrated to the extracellular level (thereby making the reversal potential of $GABA_A$ receptor-mediated inhibition equal to that of excitation). Although it is possible that different species use different mechanisms or sites to produce directional selectivity in the retina, the following points challenge this interpretation.

The finding of an increase in synaptic current asymmetry as the holding potential was raised suggested that the inhibitory input to the ganglion cell was larger in the NULL direction. Although consistent with the inhibitory-NULL presynaptic model (assuming statistical significance), it was not demonstrated whether this input was sufficient to account for the directionality. In addition, without a measurement of either the total conductance or explicit estimation of excitatory and inhibitory inputs, this result could not be tested against the excitatory-PREF presynaptic model. Likewise, at least one of these measures is required to provide direct evidence for a postsynaptic excitatory–inhibitory correlative interaction.

This study assumed that the Cl^- loading protocol simply transformed all inhibitory inputs to excitatory ones, leaving the original excitatory inputs unchanged. If this were the case, the postsynaptic correlation model predicts that the PREF and NULL responses of the now completely 'excitatory' current would have different peaks and durations, in precisely the same manner as for the overall conductance modulation G(*t*). Indeed, both presynaptic models also predict a PREF/NULL difference for the transformed synaptic responses, and therefore, the reported result of identical voltage-clamp currents is difficult to reconcile with any of the circuit models. This suggests that the effect (and thus the interpretation) of the high intracellular Cl^- may be more complex. Nevertheless, it will be important in both the turtle and rabbit to exploit the pharmacological protocols described in this

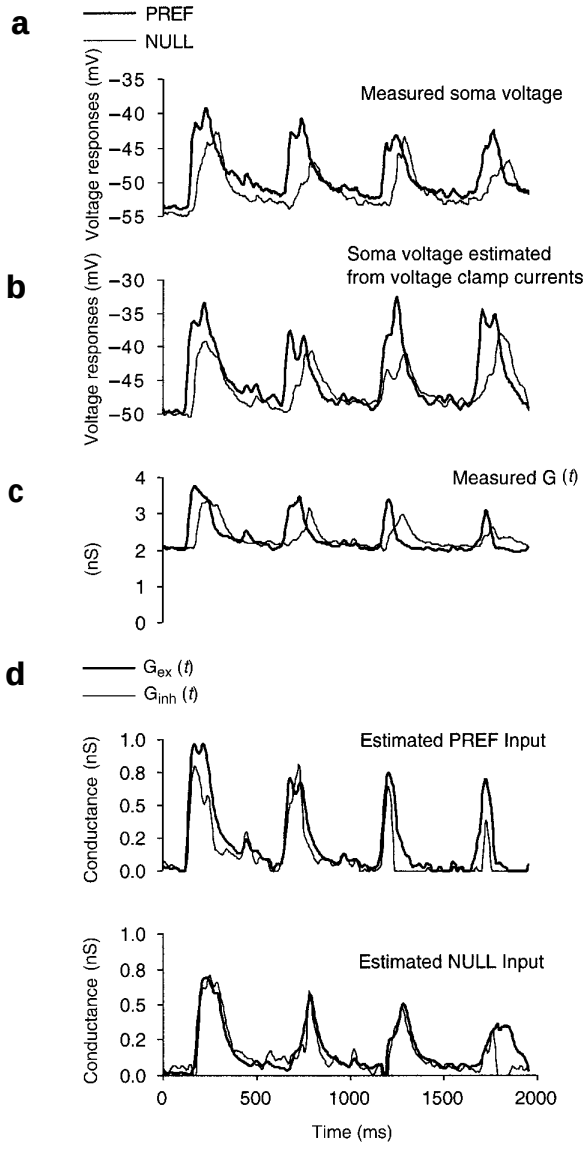

Fig. 5. Electrophysiological recordings of visual responses of a directionally selective ganglion cell (A46) in turtle retina. Voltage responses (grating stimulus with a temporal frequency of 2 Hz, 200 μm aperture, 200 μm spatial period) from current-clamp recordings (**a**) and reconstruction from voltage-clamp recordings (**b**), with the PREF and NULL directions of 90° and 270°, respectively. (**c**) The somatic input conductance G(*t*) derived from voltage-clamp traces (V_h = –45 and –90 mV) low-pass filtered at 200 Hz. G(*t*) has a larger peak for the PREF response (D_{G^*} = 0.09, with peak relative conductance 75% greater than G_0); the average conductance inputs are the same for the PREF and NULL responses, and are longer for the NULL response (D_T = –0.14). (**d**) Excitatory and inhibitory components of G(*t*). The peak values of both inputs are larger for the PREF response (D_{G^*ex} = 0.17, D_{G^*inh} = 0.07). The average of the excitation is larger for the PREF response, whereas the average inhibition is larger for the NULL response (D_{Gex} = 0.08, D_{Ginh} = –0.09). Two trials were conducted for each of the current- and voltage-clamp recordings. The time constant of decay for the voltage traces was between two and four times slower than those for the G(*t*) traces (**a**, τ_{PREF} = 3.2 s, *r* = –0.999; τ_{NULL} = 2.9 s, *r* = –0.89; **b**, τ_{PREF} = 5.7 s, *r* = –0.64; τ_{NULL} = 1.5 s, *r* = –0.26; **c**, τ_{PREF} = 0.9 s, *r* = –0.998; τ_{NULL} = 1.4 s, *r* = –0.953). In addition, the excitatory component $G_{ex}(t)$ of the G(*t*) traces decayed about two to three times more slowly than the inhibitory component $G_{inh}(t)$ (**d**, PREF, τ_{Gex} = 1.2 s, *r* = –0.997; τ_{Ginh} = 0.6 s, *r* = –0.98; **d**, NULL, τ_{Gex} = 3.1 s, *r* = –0.91; τ_{Ginh} = 0.9 s, *r* = –0.94). Time constants for the trace decays were estimated by linear fit to log integral of each response cycle minus resting value; *r* values are given for linear fit.

paper[19] (tetrodotoxin and Cs^+ loading) to strengthen the assumptions of the linear analysis I have described here.

Implications for circuitry

In which cells, then, if not in the ganglion cells, does the computation of directional selectivity occur? Indeed, in the turtle retina, intracellular responses that depend on motion direction have been found in amacrine, bipolar, horizontal and photoreceptor cells[20,21].

Although recordings presented here and elsewhere[19,22] demonstrate a shunting inhibitory input directly to the ganglion cell, an excitatory directionally selective input suggests that the $GABA_A$ receptor crucial for directional selective is not located at this cell. We previously described a model for the presynaptic generation of the directionally selective signal[23] that focused on synaptic integration within the dendrites of, especially (though not exclusively), the cholinergic starburst amacrine cell. Despite this cell's radial symmetry, it may be involved in directional selectivity because of its close anatomical relationship with directionally selective ganglion cells[24], and because of the strong dependence of directional selectivity on a cholinergic pathway[25]. In particular, the model predicts that the location of the $GABA_A$ receptor important for directional selectivity is on the dendrites of these cells, a prediction supported by the finding that GABA can directly inhibit cholinergic release from starburst amacrine cells in the rabbit[26,27].

This model can be easily adapted to the finding of directionally selective inhibition onto ganglion cells. The rabbit retina starburst cell releases GABA in addition to acetylcholine[28], and it has been suggested[29] that both outputs may be involved in directional selectivity. The somewhat counterintuitive suggestion from the findings presented here would be that a directionally selective co-release of GABA onto the same ganglion cell receiving the directionally selective acetylcholine output would not be involved in directional selectivity *per se*, but would serve a parallel function in regulating the overall output of the target ganglion cell.

In developmental terms, an advantage of this model is that classical Hebbian mechanisms[30] could be invoked to achieve mature connectivity, because the directional tuning of excitatory afferents from amacrine cells could be directly correlated with the tuning of the target ganglion cell[23]. I propose that an asymmetric connectivity of GABAergic synapses between amacrine and ganglion cells, similar to the excitatory pathway, could arise by their 'piggybacking' alongside the sharpening of the excitatory connections.

A final conclusion for neural computation arises from the finding that retinal neurons presynaptic to ganglion cells (particularly, starburst amacrine cells in the rabbit retina)[31] do not generally rely on action potentials[32]. Thus, the finding that directional selectivity is generated before the ganglion cell provides direct evidence of a functional nonlinear computation in the central nervous system that does not require the spike threshold.

Methods

Electrophysiology. Whole-cell patch recordings were taken at room temperature under low-power infrared illumination from ganglion cells in untreated intact isolated turtle retina (*Pseudemys scripta elegans*), bathed in standard Ringer's solution. (Tissue preparation, data collection and

stimulus details were described previously[11].) Animal handling and tissue acquisition protocols were approved by the Massachusetts Institute of Technology Division of Comparative Medicine. Results presented here are from 85 cells, of which 36 were analyzed for visual responses. Patch electrodes (5 MΩ) were filled with 90 mM KCH_3SO_4, 5 mM $NaCH_3SO_4$, 12 mM $MgCl_2$, 1 mM $CaCl_2$, 11 mM EGTA, 5 mM HEPES, 2 mM glucose, titrated with KOH to a pH of 7.4. There was no correction for the electrode offset (estimated at 5–10 mV). The lack of ATP in the electrode solution may have contributed to a rundown of the $GABA_A$ receptor-mediated response[33]. Nevertheless, the retinal responses showed clear inhibitory conductance changes. In particular, extrapolations of the largest peaks in phase plots of $G(t)$ versus $E_{rev}(t)$ often converged near the reversal potential of $GABA_A$ receptor channels (–60 to –70 mV), similar to what is observed in neurons in visual cortex *in vivo*[14]. Recording times for quantitative analysis of visually evoked conductance changes averaged about one to two hours. Conductance-derived measurements were taken from 19 cells, and voltage-clamp currents were examined in 34 cells (17 of which were also used for the conductance measurements).

Receptive field properties were generally assessed from extracellular spikes in on-cell mode, after which whole-cell access was obtained to make conductance measurements under either voltage or current clamp. Passive properties ($n = 59$) were $R_{in} = 870 \pm 90$ MΩ, $\tau_0 = 56 \pm 3$ ms, and $E_{rest} = -56 \pm 1$ mV. Compensation for the access resistance (between 10 and 30 MΩ), which would otherwise reduce the measured conductance changes (estimated at less than 10%), was not necessary because of the cells' high input resistance.

Directional selectivity was defined as a statistically significant difference (t-test, $p < 0.01$) between the cumulative spike count over stimuli with directions within 22.5° of a reference direction, and their opposite trajectories. Stimuli were either moving square-wave gratings ($n = 6$ and 4 for voltage clamp and conductance measurements, respectively; 100 to 400 μm spatial period, 1 to 4 Hz temporal frequency, 200 to 400 μm aperture centered over the receptive field), or light bars (300 by 200 μm) and squares (100, 200 or 300 μm) moving from 1 to 4 μm/ms along a 1000-μm path length ($n = 27$ and 15 for voltage clamp and conductance measurements, respectively). There was no clear difference in the PREF/NULL synaptic relationships between the stimulus types, contrary to suggestions for distinct stimulus-dependent directional selectivity mechanisms[7].

Voltage-clamp traces for the direct estimation of excitatory input ($I(t)$) were analyzed at holding potentials, V_h, between –80 and –120 mV (average, –93 mV). $G(t)$, $E_{rev}(t)$ and reconstructions of current-clamp voltage traces were derived using variations on a previously described method[14]. In two cases, the measurements were derived from subthreshold responses under two current-clamp conditions (holding currents of 0, between –30 and –50 pA). In four cases, a subthreshold current- clamp response was compared with a voltage-clamp recording, at a V_h between –80 and –100 mV, with the voltage-clamp current adjusted to account for the cell's input capacitance. In the remaining 13 cases, $G(t)$ and $E_{rev}(t)$ were derived from voltage-clamp recordings at two holding potentials (V_h typically –60 and –90 mV), as previously described[14]. Results presented in Fig. 4 are from traces that were low-pass filtered at 50 Hz. All quantitative measures of synaptic input were made with averages of two to eight traces (typically four) of each recording condition.

The conductance measurement allows a reconstruction of the current-clamp response without action potentials[14]. This analysis gave average values for the peak of the PREF and NULL EPSPs, V_P and V_N, respectively, as 14.8 ± 0.39 mV and 9.4 ± 0.16 mV, respectively. The PREF and NULL durations of $G(t)$ (G_0 subtracted), T_P and T_N, were calculated based on their autocorrelation functions, R (ref. 34), giving the following equation (**Figs. 2f** and **3f**).

$$T = \int_{t=-\infty}^{\infty} R(t)/R(0)$$

This derivation allows an objective estimation of signal duration, without relying on measurement of the peak response or the necessarily *ad hoc* definition of response start and end.

The index of directionality, D (**Table 1** and **Fig. 4**), for a given measure x was given by the following equation.

$$D_x = (x_P - x_N)/(x_P + x_N)$$

Here, x_P and x_N apply to the PREF and NULL responses, respectively. All measures were subtracted from their resting values (the differences were always greater than 0), with PREF and NULL directions defined by the spike response. In Table 1, p values for the D measures are for significance given by the Wilcoxon two-tailed signed-ranks test on the set of paired measures [x_P, x_N].

Dissection of the excitatory and inhibitory components of the synaptic input from the measured $G(t)$ and $E_{rev}(t)$ were made with the following formulas (C. Monier *et al. Soc. Neurosci. Abstr.* **24**, 354.3, 1998).

$$G_{inh}(t) = (G(t) - G_0)\,(E_{ex}(t) - E_{rev}(t)) / (E_{ex}(t) - E_{inh}(t))$$
$$G_{ex}(t) = (G(t) - G_0)\,(E_{rev}(t) - E_{inh}(t)) / (E_{ex}(t) - E_{inh}(t))$$

Here, $E_{ex}(t)$ is given by maximum ($E_{rev}(t)$, 20 mV), and $E_{inh}(t)$ by minimum ($E_{rev}(t)$, –70 mV). This derivation assumes a simple single compartment circuit of the neuron consisting of a leak conductance (G_0), and excitatory ($G_{ex}(t)$) and inhibitory ($G_{inh}(t)$) synaptic conductances connected in parallel, each in series with their associated reversal potentials ($E_{ex}(t)$ and $E_{inh}(t)$, respectively, for the synapses).

Simple neuron model predictions. Steady state minimum synaptic conductance modulations for the simple isopotential neuron model were given by the following formulas.

$$G_{ex} = (G_0 \times V_P) / (E_{ex} - E_{rest} - V_P)$$
$$G_{inh} = ((G_0 \times V_N) + G_{ex}(V_N - E_{ex} + E_{rest})) / (E_{inh} - E_{rest} - V_N)$$

E_{rest} and E_{inh} were set to –70 mV, E_{ex} = 0 mV, V_P = 15 mV and V_N = 10 mV. These equations are divided through by G_0, thereby giving relative values of G_{ex} and G_{inh} of 27% and 64%, respectively. Thus, the peak conductance during the NULL response of either the inhibitory-NULL or postsynaptic model should be at least 190% of G_0. Furthermore, the lowest peak conductance change for the postsynaptic model PREF response will given by a completely uncorrelated inhibitory input, thus 160% of G_0. This calculation also suggests that the minimum peak conductance modulation during the PREF response of the excitatory-PREF model will be 130%, that is, when there is no inhibitory input.

Computer simulations. The detailed model is based on a 179 compartment reconstruction (**Fig. 2c**) of a turtle retina ganglion cell (type G20, Fig. 16a in ref. 35). This anatomical type has been associated with the directional selective physiological type[21,36]. Assuming a membrane capacitance of 0.7 μF/cm^2, the membrane resistivity was chosen to give a membrane time constant that matched the data (56 ms). With the intracellular resistivity, R_i, set to 200 Ω•cm, the resulting input resistance, R_{in}, was 470 MΩ. The reversal potential for the membrane leak resistance was –70 mV. Each compartment had identical pairs of excitatory and inhibitory synapses with temporal impulse responses given by the difference of two exponentials (0.5 and 2, 0.5 and 5 ms, respectively) multiplied by a scaling coefficient, with reversal potentials of 0 and –70 mV, respectively. The 0.40 ratio of the second pair of time constants is consistent with the generally faster kinetics of excitatory versus inhibitory synapses (but see below). The spatial receptive field for all synapses was a unit impulse (equal to one if the stimulus illuminated the synapse, and equal to zero if otherwise), and activation of the synapses was equivalent to a one-dimensional impulse (edge) moving at 4 μm/ms across the receptive field.

The extreme minimal values in both space and time for the synaptic properties were chosen for two reasons. First, these limits emphasized the relationship between relative synaptic delays and the NULL direction correlation underlying the postsynaptic model, by allowing a maximum sensitivity to input correlations. Second, and more fundamentally, a goal of the simulations was to derive lower bounds on the net conductance modulations; increasing either the synaptic time constants or enlarging the spatial receptive fields would inevitably increase these minimum values.

The passive dendritic model ignores the evidence for voltage-dependent channels in dendritic trees (for example, in retinal ganglion cells[37]). However, the passive model was chosen because of its simplicity, to get first-order estimates of the modulation due to synaptic input alone, in particular lower bounds on these modulations. Systematic model simulations exploring the effect of nonlinear dendritic membrane properties will be important, but are beyond the scope of this article.

As with the simple model, synaptic strengths were chosen to reproduce the above values for V_P and V_N (**Fig. 2a**) using the minimum

amount of synaptic input, and thus to provide a lower bound for measurements of input conductance modulation. First, the excitatory strength was adjusted to obtain a maximum response V_P with no inhibition. The inhibitory strength was then adjusted to reduce the excitation-only response to V_N when there was zero relative delay between synapses at a given node; this condition was defined as the NULL response. These constraints gave scaling coefficients of 0.3 and 0.2 nS for each excitatory and inhibitory synapse, respectively. With all synapses active, an overall delay (dT) of at least 100 ms between each pair of synapses, defined as the PREF response, was necessary to recover V_P (inhibition following excitation; simulations with inhibition preceding excitation by 100 ms gave similar results; **Fig. 2e**).

With respect to the postsynaptic circuit shown in Fig. 1, these parameters give values for the spatial separation d*x* and the intrinsic delay in the inhibitory pathway d*t*, as follows. The overall delay dT between the arrival of excitation and inhibition at the ganglion cell for the PREF and NULL responses is given by the sum and difference, respectively, of d*t* and the time for a stimulus of velocity *V* to travel a distance d*x* along the retinal surface between the two inputs. The maximum correlation between excitation and inhibition at the ganglion cell for the NULL direction response occurs when dT = 0, giving the following equation.

$$dx/V = dt$$

For the PREF response, then, the following equation applies.

$$dT = dx/V + dt$$

Thus, a stimulus velocity of 4 μm/ms and an overall delay of 100 ms for the PREF response yields values of 200 μm for d*x* and 50 ms for d*t*.

The sub-linear integration of synaptic inputs on a passive dendritic tree will tend to underestimate the actual conductance inputs as derived from somatic measurements. For the postsynaptic model, the underestimation of the area will be worse for the NULL response because of synaptic shunting, making the associated directional index *D* non-zero and positive, and likewise will reduce the asymmetry of the peak response. This effect can be demonstrated by comparing simulations with the normal value for R_i (200Ω•cm) as well as the 'ideal' case with $R_i = 0$ (data not shown). For the average responses of G(*t*) and I(*t*), the effect of this distortion is relatively small, and it does not cause the index of any of the measures to switch sign.

Simulations of somatic voltage clamp used an ideal voltage clamp algorithm[38]. Simulations were run with the Surf-Hippo system (www.cnrs-gif.fr/iaf/iaf9/surf-hippo.html, code available from the author).

Acknowledgements

I thank T. Poggio for support and inspiration for this project, and for providing his laboratory for the experiments (Department of Brain and Cognitive Science at the Massachusetts Institute of Technology). I also thank L. Menendez de la Prida for comments on the manuscript, N. Grzywacz and R. Smith for technical assistance and discussions at an early stage of the work, and J. Lisman, E. Fernandez, J. Ammermuller, Y. Frégnac, C. Monier, V. Bringuier and I. Segev for discussions. Part of this work was supported by grants from the Fondation Fyssen, Fondation Phillipe, and a CNRS ATIPE Fellowship.

Received 13 September 2000; Accepted 2 January 2001

1. Maturana, H. R., Lettvin, J. Y., McCulloch, W. S. & Pitts, W. H. Anatomy and physiology of vision in the frog (*rana pipiens*). *J. Gen. Physiol*. **43 (Suppl. 2)**, 129–171 (1960).
2. Vaney, D. I., He, S., Taylor, W. R. & Levick, W. R. in *Computational, Neural and Ecological Constraints of Visual Motion Processing* (eds. Zanker, J. & Zeil, J.) 2–44 (Springer, Berlin, 2000).
3. Barlow, H. B. & Levick, W. R. The mechanism of directionally selective units in rabbit's retina. *J. Physiol. (Lond.)* **178**, 477–504 (1965).
4. Koch, C., Poggio, T. & Torre, V. Retinal ganglion cells: a functional interpretation of dendritic morphology. *Phil. Trans. R. Soc. Lond. B Biol. Sci.* **298**, 227–264 (1982).
5. Yang, G. & Masland, R. H. Receptive fields and dendritic structure of directionally selective retinal ganglion cells. *J. Neurosci.* **14**, 5267–5280 (1994).
6. He, S. & Masland, R. H. Retinal direction selectivity after targeted laser ablation of starburst amacrine cells. *Nature* **389**, 378–382 (1997).
7. Grzywacz, N. M., Amthor, F. R. & Merwine, D. K. Necessity of acetylcholine for retinal directionally selective responses to drifting gratings in rabbit. *J. Physiol. (Lond.)* **512**, 575–581 (1998).
8. He, S., Jin, Z. F. & Masland, R. H. The nondiscriminating zone of directionally selective retinal ganglion cells: comparison with dendritic structure and implications for mechanism. *J. Neurosci*. **19**, 8049–8056 (1999).
9. Caldwell, J. H., Daw, N. W. & Wyatt, H. J. Effects of picrotoxin and strychnine on rabbit retinal ganglion cells: lateral interactions for cells with more complex receptive fields. *J. Physiol. (Lond.)* **276**, 277–298 (1978).
10. Ariel, M. & Adolph, A. R. Neurotransmitter inputs to directionally sensitive turtle retinal ganglion cells. *J. Neurophysiol*. **54**, 1123–1143 (1985).
11. Smith, R. D., Grzywacz, N. M. & Borg-Graham, L. Is the input to a GABAergic synapse the sole asymmetry in turtle's retinal directional selectivity? *Vis. Neurosci*. **13**, 423–439 (1996).
12. Massey, S. C., Linn, D. M., Kittila, C. A. & Mirza, W. Contributions of $GABA_A$ receptors and $GABA_C$ receptors to acetylcholine release and directional selectivity in the rabbit retina. *Vis. Neurosci.* **14**, 939–948 (1997).
13. Poggio, T. & Reichardt, W. E. Considerations on models of movement detection. *Kybernetik* **13**, 223–227 (1973).
14. Borg-Graham, L., Monier, C. & Frégnac, Y. Visual input evokes transient and strong shunting inhibition in visual cortical neurons. *Nature* **393**, 369–373 (1998).
15. Torre, V. & Poggio, T. A synaptic mechanism possibly underlying directional selectivity to motion. *Proc. R. Soc. Lond. B Biol. Sci.* **202**, 409–416 (1978).
16. Koch, C., Douglas, R. & Wehmeier, U. Visibility of synaptically induced conductance changes: theory and simulations of anatomically characterized cortical pyramidal cells. *J. Neurosci.* **10**, 1728–1744 (1990).
17. Spruston, N., Jaffe, D. B., Williams, S. H. & and Johnston, D. Voltage- and space-clamp errors associated with the measurement of electrotonically remote synaptic events. *J. Neurophysiol.* **70**, 781–802 (1993).
18 Rodieck, R. W. *The Vertebrate Retina* (Freeman, San Francisco, 1973).
19. Taylor, W. R., He, S., Levick, W. R. & Vaney, D. I. Dendritic computation of direction selectivity by retinal ganglion cells. *Science* **289**, 2347–2350 (2000).
20. DeVoe, R. D., Carras, P. L., Criswell, M. H. &. Guy, R. G. in *Neurobiology of the Inner Retina* (eds. Weiler, R. & Osborne, N. N.) 235–246 (Springer, Berlin, 1989).
21. Ammermuller, J., Muller, J. F. & Kolb, H. The organization of the turtle inner retina. II. Analysis of color-coded and directionally selective cells. *J. Comp. Neurol.* **358**, 35–62 (1995).
22. Marchiafava, P. L. Centrifugal actions on amacrine and ganglion cells in the retina of the turtle. *J. Physiol. (Lond.)* **255**, 137–155 (1976).
23. Borg-Graham, L. & Grzywacz, N. M. in *Single Neuron Computation* (eds. McKenna, T., Davis, J. & Zornetzer, Z. F.) 347–376 (Academic, San Diego, 1992).
24. Vaney, D. I., Collin, S. P. & Young H. M. in *Neurobiology of the Inner Retina* (eds. Weiler, R. and Osborne, N. N.) 157–168 (Springer, Berlin, 1989).
25. Masland, H., Mills, J. W. & Cassidy, C. The function of acetylcholine in the rabbit retina. *Proc. R. Soc. Lond. B Biol. Sci.* **223**, 121–139 (1984).
26. Linn, D. M. & Massey, S. C. GABA inhibits ACh release from the rabbit retina: A direct effect or feedback to bipolar cells? *Vis. Neurosci*. **8**, 97–106 (1992).
27. Zhou, J. Z. & Fain, G. L. Neurotransmitter receptors of starburst amacrine cells in rabbit retinal slices. *J. Neurosci.* **15**, 5334–5345 (1995).
28. O'Malley, D. M., Sandell, J. H. & Masland, R. H. Co-release of acetylcholine and GABA by the starburst amacrine cells. *J. Neurosci.* **12**, 1394–1408 (1992).
29. Vaney, D. in *Progress in Retinal Research* vol. 9 (eds. Osborne, N. & Chader, G.) 49–100 (Pergamon, New York, 1990).
30. Brown, T. H., Kairiss, E. W. & Keenan, C. L. Hebbian synapses: biophysical mechanisms and algorithms. *Annu. Rev. Neurosci.* **13**, 475–511 (1990).
31. Peters, B. N. & Masland, R. H. Responses to light of starburst amacrine cells. *J. Neurophysiol.* **75**, 469–480 (1996).
32. Dowling, J. E. *The Retina, an Approachable Part of the Brain* (Harvard Univ. Press, Cambridge, Massachusetts, 1987).
33. Stelzer, A., Kay, A. R. & Wong, R. K. S. GABA-A-receptor function in hippocampal cells is maintained by phosphorylation factors. *Science* **241**, 339–341 (1988).
34. Siebert, W. *Circuits, Signals, and Systems* (MIT Press, Cambridge, Massachusetts, 1986).
35. Kolb, H. The morphology of the bipolar cells, amacrine cells and ganglion cells in the retina of the turtle pseudemys scripta elegans. *Phil. Trans. R. Soc. Lond. B Biol. Sci.* **298**, 355–393 (1982).
36. Jensen, R. J. & DeVoe, R. D. Comparisons of directionally selective with other ganglion cells of the turtle retina: intracellular recording and staining. *J. Comp. Neurol.* **217**, 271–287 (1983).
37. Velte, T. J. & Masland, R. H. Action potentials in the dendrites of retinal ganglion cells. *J. Neurophysiol.* **81**, 1412–1417 (1999).
38. Borg-Graham, L. Additional efficient computation of branched nerve equations: adaptive time step and ideal voltage clamp. *J. Comp. Neurosci.* **8**, 209–225 (2000).